Acoustic Vector Network Analysis

by

M. C. Wittmann

A thesis submitted to the

Faculty of the School of Arts & Sciences of the

University of Colorado in partial fulfillment

of the requirements for the degree of

Bachelor of Arts

Department of Physics

2009

This thesis entitled:
Acoustic Vector Network Analysis
written by M. C. Wittmann
has been approved for the Department of Physics

_____

John Price

_____

John Cumalat

_____

Stephen Preston

Date _____

Wittmann, M. C. (B.A., Physics)

Acoustic Vector Network Analysis

Thesis directed by Prof. John Price

Acoustic vector network analysis is the acoustic analog of a measurement system commonly used in microwave electronics. Vector network analysis (VNA) allows for a complete characterization of an object's acoustic properties. Using this technique, one can determine the acoustic power reflected and transmitted from an object (the test device, using terminology from microwave network analysis) as well as the phase shift of reflected and transmitted waves. In this way we may determine the complex-valued components of the test device's scattering matrix. This allows for the characterization of acoustic elements in a way analogous to electronic circuit elements, in terms of the acoustic analogs of resistance and reactance.

As a first experiment I apply single-port VNA to the analysis of an acoustic resonating cavity. I show how the measured reflection coefficient can be used to characterize the resonances of the cavity. Experimental results are compared with theory and numerical simulation, which show good agreement.

I also describe a method for extending our AcousticVNA hardware and software to enable two-port acoustic measurements. I discuss calibration and wave-fitting methods and give an algorithm for two-port scattering matrix calculation.

Dedication

To my parents, for their endless love and support.

Acknowledgements

I would like to thank John Price for his guidance and support, without which this project would not have been possible; John Cumalat for running a top-notch honors class and always being available and happy to help; Stephen Preston for teaching me numerical analysis (and still being willing to sit on my honors committee); Daniel and Justin for comradery in the acoustics lab; Stephen and Jessica for keeping me on track and supporting me at my defense; my parents for pep talks and support at every step of the way; the faculty, staff, and Class of 2009 of the University of Colorado Physics Department for making the last four years an incredible experience.

Contents

Chapter

Tables

Table

Figures

Figure

Chapter 1

Introduction

1.1 What is Acoustic Vector Network Analysis?

In electronics, the **network analyzer** is a powerful measurement tool indispensable in microwave circuit analysis.

A network analyzer characterizes the relationship between the amplitude of an input signal and the amplitude of resulting output signals at one or more points (called **ports**) in a network of components (or **test device**). A **vector network analyzer** (VNA) is capable of measuring complex amplitude ratios (which include magnitude and phase), hence the "vector" prefix.

Vector network analyzers work by measuring the amplitudes of incident (propagating toward the device) and emergent (propagating away from the device) modes at each port. The quantity of interest is the **scattering matrix**, defined as the matrix that transforms a vector of incident amplitudes into a vector of emergent amplitudes. For example, in a two-port system, if we denote the amplitudes of the incident and emergent modes at the first port a_1 and b_1 and the same quantities at the second port a_2 and b_2, then the four elements of the scattering matrix are defined by

$$\begin{pmatrix} b_1 \\ b_2 \end{pmatrix} = \begin{pmatrix} s_{11} & s_{12} \\ s_{21} & s_{22} \end{pmatrix} \begin{pmatrix} a_1 \\ a_2 \end{pmatrix}.$$

Note that when there is no incident wave in the second port ($a_2 = 0$), $s_{11} = b_1/a_1$ and $s_{21} = b_2/a_1$, so s_{11} is the reflection coefficient of the test device looking into the

first port and s_{21} is the transmission coefficient from the first port to the second port. Similarly (when $a_1 = 0$), s_{22} is the reflection coefficient looking into the second port and s_{12} is the transmission coefficient from the second port to the first port.

The individual elements of the scattering matrix, which represent reflection and transmission coefficients, are often referred to as **s-parameters**. For an n-port device, there are n^2 s-parameters, elements of an $n \times n$ scattering matrix.

Though vector network analysis is frequently applied to measurements of microwave networks, the concept is applicable to any system with confined waves. Acoustic vector network analysis is a direct analog—the goal is still to determine the scattering matrix of an object (or test device, carrying over terminology from microwave network analysis) but in the acoustic case we are interested the interaction of the device with sound waves, rather than electromagnetic waves.

Acoustic vector network analysis allows for a complete characterization of an object's acoustic properties. Using this technique, one can determine the power reflected and transmitted by an acoustic component, as well as phase shift of reflected and transmitted waves. This allows the characterization of acoustic elements in a way analogous to electronic circuit elements, in terms of the acoustic analogs of resistance and reactance.

1.2 Applications

In a single-port configuration, an acoustic vector network analyzer can be used to measure the reflection coefficient of an acoustic component attached to a waveguide. The reflection coefficient—the ratio of the complex amplitude of the incident signal to the complex amplitude of the reflected signal—is a useful quantity in acoustic analysis.

For example, measurements of the reflection coefficient of a horn attached to an acoustic waveguide can be used to characterize the radiation efficiency of the horn.[1] In

[1] Assuming negligible mechanical losses

the frequency range where the horn is designed to operate, we would expect the reflection coefficient to be small, so that most of the incident power is radiated away. Precise measurements of the reflection coefficient may be used to characterize and improve the performance of horns and other acoustic components.

Such measurements are also valuable in the field of musical acoustics. For example, measurements of the reflection coefficient of components of wind instruments such as the recorder have been used to study the mechanism of air-jet amplification and forked fingering patterns [6, 11].

The reflection coefficient of an acoustic resonator such as a cavity resonator (see Chapter 4) can be used to determine resonant frequencies and characterize behavior at resonance. Such information is invaluable in many fields of engineering, from the design of audio equipment to architectural acoustics [10].

Two-port measurements allow characterization of transmission as well as reflection coefficients. Measurements of this kind are useful in the characterization of the absorption properties of solid materials, for example, sound absorbing tiles or vibration-damping materials. For such applications it is desirable to find materials that minimize power reflected and transmitted (and thus maximize power absorbed) in a desired frequency range.

Chapter 2

Background

In this chapter I give a brief introduction to the concepts and mathematics useful in acoustic waveguide analysis.

2.1 The Helmholtz Equation

Sound is transmitted in a medium by the propagation of pressure variations. The difference between the pressure at a point and the average (or **quiescent**) pressure is called **acoustic pressure**, hereafter denoted by p. It can be shown [8] that if the acoustic pressure p is small relative to the quiescent pressure, then $p(\mathbf{r})$ obeys the wave equation:

$$\nabla^2 p = \frac{1}{c^2}\frac{\partial^2 p}{\partial t^2}, \tag{2.1}$$

where c is the speed of sound in the medium.

We will usually be interested in solutions with sinusoidal time dependence,

$$p(\mathbf{r}, t) = p(\mathbf{r}) \exp(-i\omega t), \tag{2.2}$$

though we may use the tools of Fourier analysis to construct a general solution from solutions with sinusoidal time dependence. Inserting (2.2) into (2.1) gives, with the definition $k = \omega/c$,

$$\left(\nabla^2 + k^2\right) p(\mathbf{r}) = 0. \tag{2.3}$$

This is the Helmholtz equation, the partial differential equation that describes the spatial dependence of solutions of the wave equation with sinusoidal time dependence. It is a common starting point for problems in acoustics.

2.2 Acoustic Waveguides

2.2.1 Separation of the Helmholtz Equation

In the analysis of a cylindrical waveguide oriented in the z direction, we will be interested in solutions to the Helmholtz equation of the form [4]

$$u(\mathbf{r}) = f(\mathbf{R})\, g(z), \tag{2.4}$$

where $\mathbf{R}$ represents the coordinates in the transverse (yz) plane. Inserting (2.4) into the Helmholtz equation and dividing by fg, we obtain the separated equation

$$-\frac{1}{f}\nabla^2 f = \frac{1}{g}g'' + k^2 = K^2, \tag{2.5}$$

where K^2 is the separation constant. We obtain the equations

$$g'' = -\gamma^2 g \tag{2.6}$$

$$0 = \nabla^2 f + K^2 f, \tag{2.7}$$

where $\gamma = \sqrt{k^2 - K^2}$ is the **propagation constant**. Assuming that K^2 is positive[1] , γ will be positive real or positive imaginary.

The general solution of (2.6) is

$$g(z) = a\exp(i\gamma z) + b\exp(-i\gamma z). \tag{2.8}$$

The first term on the right represents a wave that propagates or decays in the $+z$ direction, while the second term represents a wave that propagates or decays in the $-z$ direction.

[1] This assumption is necessary to ensure physically realizable solutions. The resulting basis is complete, allowing for the construction of a general solution.

2.2.2 Solutions in cylindrical coordinates

The solution of f depends on the geometry of the waveguide. In cylindrical coordinates,

$$\nabla^2 f = \frac{1}{r}\frac{\partial}{\partial r}\left(r\frac{\partial f}{\partial r}\right) + \frac{1}{r^2}\frac{\partial^2 f}{\partial \varphi^2} + \frac{\partial^2 f}{\partial z^2}. \tag{2.9}$$

We will be interested in separable solutions of the form

$$f(\mathbf{R}) = R(r)\,\Phi(\varphi). \tag{2.10}$$

Substituting (2.9) and (2.10) into (2.7) and multiplying by $r^2/R\Phi$ yields the separated equation

$$-\frac{1}{\Phi}\Phi'' = \frac{r}{R}\left(R' + rR''\right) + r^2K^2 = m^2,$$

where m^2 is the separation constant. We obtain the equations

$$\Phi'' = -m^2\Phi \tag{2.11}$$

$$0 = r^2R'' + rR' + \left(r^2K^2 - m^2\right)R. \tag{2.12}$$

The general solution of (2.11) is

$$\Phi(\varphi) = c\exp(im\varphi) + d\exp(-im\varphi). \tag{2.13}$$

We restrict our interest to solutions that are single-valued (i.e. 2π periodic in φ), requiring that m is an integer.

The second equation (2.12) is Bessel's equation of order m. The general solution is a superposition of J and Y Bessel functions. Here we restrict our interest to solutions that are finite at $r = 0$, and thus we may discard the Y term:

$$R(r) = J_m(Kr) = J_m\left(r\sqrt{k^2 - \gamma^2}\right). \tag{2.14}$$

Equations (2.4) and (2.10), together with (2.8), (2.13), and (2.14), give a specific solution of the Helmholtz equation in free space. The general solution is a superposition of these specific solutions.

2.2.3 Boundary conditions

In order to solve the Helmholtz equation in a confined volume such as a waveguide, we must develop a theory of the behavior of the pressure field at a boundary. For our purposes, we need only to consider hard surface boundaries.

When effects of viscosity can be ignored, an appropriate model is the **sliding boundary condition**, in which only the perpendicular component of the fluid velocity must vanish at a surface. Because velocity is proportional to the pressure gradient, we can write this as

$$\mathbf{n} \cdot \nabla p = 0 \text{ at a hard surface,} \tag{2.15}$$

where $\mathbf{n}$ is a vector normal to the surface.

In reality, molecular scattering from surfaces is generally diffuse, meaning that the average (fluid) velocity is zero at a surface. Were we using a more sophisticated model (such as the Navier-Stokes equations, which model viscosity), we should really enforce that **all** components of the velocity vanish at a surface. However, this condition would produce non-physical solutions if applied to the wave equation, which does not model viscosity. Furthermore, taking viscosity into account, it can be shown that the effect of diffuse scattering is only significant in a thin region known as the **viscous penetration depth**, δ_s. At a distance δ_s from a surface, the sliding boundary condition is an excellent approximation.

Another complication that becomes significant in a thin region near a surface is the transition of adiabatic conditions in the flow to nearly isothermal conditions at the surface. Hence, the (acoustic) pressure gradient, and with it the fluid velocity, approaches zero at a surface. However, this effect is only significant in a thin region known as the **thermal penetration depth**, δ_h [8, 12].

In the frequency range with which we will be concerned (20 Hz to 20 kHz), both δ_s and δ_h range from about half a millimeter to a hundredth of a millimeter [8], lengths

much smaller than the dimensions of the waveguides we expect to use. For the purposes of the analysis in this paper, we take the sliding boundary condition to be an excellent approximation.

2.2.4 Solutions in a circular waveguide

When applied to the case of a circular waveguide (i.e., a cylindrical waveguide with a circular cross-section) oriented along the z axis, the sliding boundary condition (2.15) introduced in the previous section requires that $\hat{\mathbf{r}} \cdot \nabla u = 0$ at $r = a$, where a is the radius of the waveguide, or, equivalently,

$$R'(a) = KJ'_m(Ka) = 0. \tag{2.16}$$

For $m = 0$, there is a nontrivial solution when $K = 0$ (or $\gamma = k$). This solution gives the mode we will label (00):

$$u_{00}^{\pm}(\mathbf{r}) = \exp(\pm ikz). \tag{2.17}$$

This mode behaves like a plane wave and propagates at all frequencies. Note that $\gamma = k$ implies that the phase velocity is equal to the free-space phase velocity of sound.

The other nontrivial solutions must have $K \neq 0$. In this case, the condition (2.16) is satisfied only if Ka is a positive root of J'_m— each root corresponds to a different mode. A general formula for the mode labeled $(m, \mu - 1)$ is

$$u_{m,\mu-1}^{\pm}(\mathbf{r}) = \exp(im\varphi)\exp(\pm i\gamma_\mu z)\, J_m\left(\frac{j'_{m\mu}}{a}r\right), \tag{2.18}$$

where

$$\gamma_\mu = \sqrt{k^2 - \left(j'_{m\mu}/a\right)^2} \tag{2.19}$$

Here $j'_{m\mu}$ denotes the μth positive root of J'_m, except when $m = 0$, in which case zero is regarded as the first root [1]. Thus μ is a positive integer.

A fundamental consequence of (2.19) is the existence of **cutoff frequencies**, or frequencies below which a given mode will not propagate. If $k < j'_{m\mu}/a$, the propagation

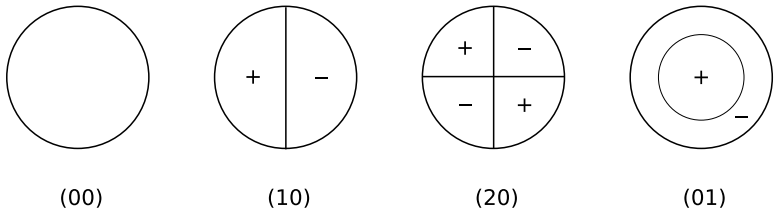

Figure 2.1: Cross-sectional shapes of the four modes of a cylindrical waveguide with the lowest cutoff frequencies

constant γ_μ becomes imaginary, leading to a solution that decays exponentially in z. Thus, the cutoff frequency of the mode $(m, \mu - 1)$ is given by

$$f_c = \frac{c}{2\pi a} j'_{m\mu}. \tag{2.20}$$

Cross sections of the four modes with the lowest cutoff frequencies are shown in Figure 2.1 and the cutoff frequencies are listed in Table 2.1. Note that the mode labeled $(m\mu)$ has m angular nodal lines (zeros) and μ radial nodal lines.

The existence of cutoff frequencies is an important result for our purposes: waveguide measurements are greatly simplified if we can assume that only the (00) mode, which behaves like a simple plane wave, is propagating. By operating at frequencies below the cutoff frequency of the (10) mode, we can ensure that only the (00) mode propagates.

Mode	$f_c \cdot \pi d/c$
00	0
10	1.841
20	3.054
01	3.832
30	4.201
40	5.318
11	5.331

Table 2.1: Cutoff frequencies for modes of a circular waveguide with diameter d

2.3 Acoustic Waveguide Measurements

The ability to measure the amplitudes of propagating modes inside a waveguide is useful in many instances. For example, such measurements allow us to characterize acoustic elements in a way analogous to electronic circuit elements, in terms of the acoustic analogs of familiar quantities in electronic circuit analysis.

All of our measurements will be conducted at frequencies below the cutoff frequency of the second mode ($\sim$ 8 kHz for our 2.5 cm diameter waveguide), so we may assume that only the (00) mode propagates. This mode is unique in that the pressure field is independent of r and φ. Thus, a pressure measurement at the wall of the waveguide determines the pressure in the entire plane perpendicular to the axis at that point.

When only the (00) mode propagates, the pressure field in the waveguide may be written as a superposition of right- and left-going plane waves (where "left" refers to the $-z$ direction and "right" refers to the $+z$ direction):

$$p(z) = a\exp(ikz) + b\exp(-ikz). \tag{2.21}$$

For the remainder of this section I implicitly assume that only the (00) mode propagates.

2.3.1 The reflection coefficient

We define reflection coefficient as the amplitude ratio of the left-going wave to the right-going wave at the **reference plane** $z = d$:

$$R(z=d) = \frac{b\exp(-ikd)}{a\exp(ikd)} = \frac{b}{a}\exp(-2ikd). \tag{2.22}$$

By calculating the reflection coefficient at a reference plane that coincides with a discontinuity in the waveguide, we may obtain a useful characterization of the discontinuity.

The two simplest waveguide discontinuities are the open (no boundary) and closed (rigid boundary) end terminations. Ideally, we expect the reflection coefficient to be -1

at an open end and 1 at a closed end. This can be understood intuitively by considering the behavior of the pressure field at each type of end boundary—at an open end, we expect a pressure minimum, which can only be achieved if the incident and reflected waves are 180 degrees out of phase at that point; at a closed end, we expect a pressure maximum, which can only be achieved if the incident and reflected waves are in phase.

The reflection coefficient not only tells us the phase shift of the reflected wave (which is useful in determining the impedance difference at a discontinuity) but also the ratio of the magnitude of the reflected wave to the incident wave. The latter can be used to determine the acoustic power reflected at a discontinuity.

2.3.2 The scattering matrix

Often in acoustic analysis we are interested not only in the way an object reflects incident sound waves, but also how it transmits or absorbs them. For a simple example, consider two identical sections of cylindrical waveguide coupled by an aperture smaller than the waveguide diameter (see Figure 2.2). A sound wave incident on the aperture from the left will produce a reflected wave in the first port and a transmitted wave in the second port. Letting a_i and b_i denote the incoming and outgoing amplitudes at the ith port, we define the **transmission coefficient** from port 1 to 2 as the amplitude ratio of transmitted wave to the incident wave:

$$s_{21}\left(z_1 = d_1, z_2 = d_2\right) = \frac{b_2 \exp\left(-ikd_2\right)}{a_1 \exp\left(ikd_1\right)} = \frac{b_2}{a_1} \exp\left[-ik\left(d_1 + d_2\right)\right]. \tag{2.23}$$

Note that s_{21} is a function of d_1, the reference plane in the first port, and d_2, the reference plane in the second port. If asymmetries are present, we might also be interested in the transmission coefficient from port 2 to port 1, given by

$$s_{12}\left(d_1, d_2\right) = \frac{b_1}{a_2} \exp\left[-ik\left(d_1 + d_2\right)\right]. \tag{2.24}$$

Using this new notation, it is natural to let s_{11} and s_{22} represent reflection coefficients looking into the first and second ports. These s coefficients are called **s-**

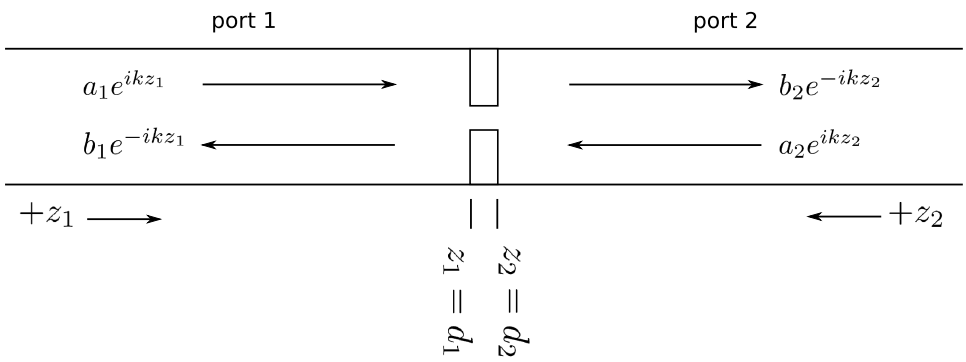

Figure 2.2: Identical sections of acoustic waveguide separated by an aperture (note that each port has its own coordinates)

parameters and are the elements of the **scattering matrix**, defined as the matrix that transforms a vector of incident amplitudes (the a's) to a vector of emergent amplitudes (b's). In this two-port example the scattering matrix is 2×2 and is defined by

$$\begin{pmatrix} b_1 \exp(-ikz) \\ b_2 \exp(-ikz') \end{pmatrix} = \begin{pmatrix} s_{11} & s_{12} \\ s_{21} & s_{22} \end{pmatrix} \begin{pmatrix} a_1 \exp(ikz) \\ a_2 \exp(ikz') \end{pmatrix}. \tag{2.25}$$

Chapter 3

AcousticVNA Hardware and Software

AcousticVNA is an inexpensive system capable of making precise acoustic waveguide measurements, developed by Dr. John Price's group at the University of Colorado at Boulder.

3.1 Apparatus

The apparatus consists of a compression driver (a type of speaker designed to feed a cylindrical waveguide) coupled to a cylindrical acoustic waveguide with six embedded electret microphones (see Figure 3.1). The microphones are connected via a set of buffer amplifiers to a digitizer, which is capable of simultaneously sampling the six channels. Control and data analysis is done in MATLAB using AVNA Lab v1.0, a software package developed by John Price's group.

In the configuration shown in Figure 3.1, AcousticVNA is capable of measuring the complex reflection coefficient of a test object, which is coupled to the microphone section at the end opposite to the compression driver.

3.2 Measurement Procedure

3.2.1 Calibration

The first step in the measurement process is the relative calibration of the microphones. AcousticVNA uses relatively inexpensive electret microphones, which are not

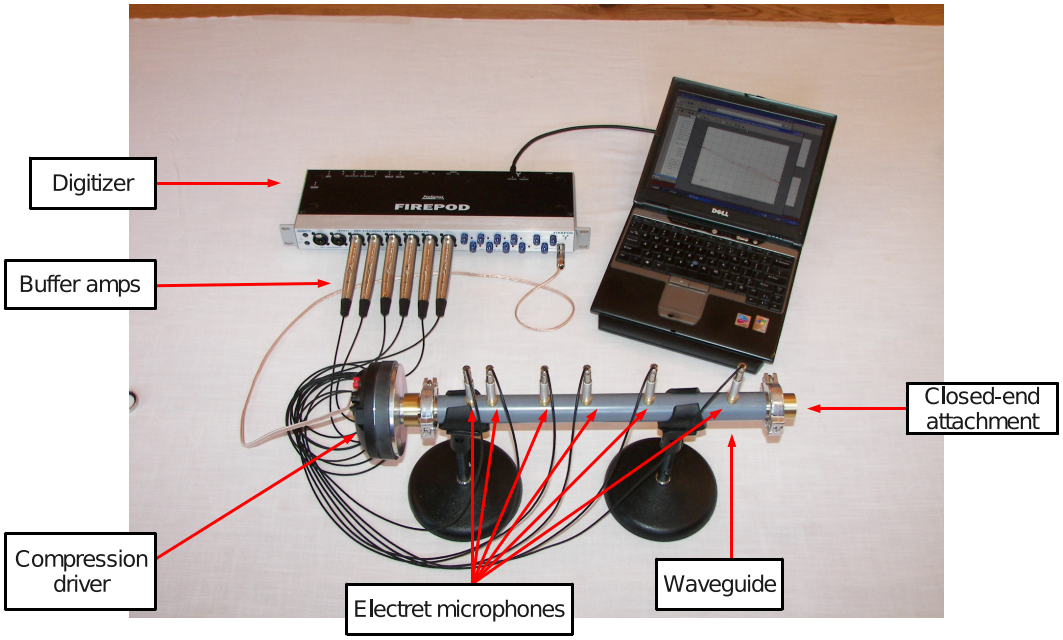

Figure 3.1: AcousticVNA hardware for single-port measurements

Figure 3.2: Microphone calibration cell used with AcousticVNA

generally provided with absolute calibration data (so we can't deduce absolute pressure amplitude from the microphone signal), and aren't necessarily stable (i.e. their responsiveness varies with temperature and time)[1] .

Fortunately, we require only **relative** microphone calibration—that is, we need to know the differences in the amplitudes and phases recorded by each microphone when they "hear" the same sound. To do this, we insert the microphones into the **calibration cell** (shown in Figure 3.2), which ensures all the microphones are subject to the same pressure field. One of the microphones is taken to be a reference, and its complex amplitude divided out of the complex amplitudes of the other microphones. The result is a set of complex amplitudes relative to the reference microphone—these amplitudes are divided out of the microphone signals to obtain calibrated data.

As the relative amplitudes may vary with frequency, the calibration process is carried out for a range of frequencies. This process is automated by the `calibrate.m` routine[2] .

[1] We assume the microphone response is linear in the operating pressure range (this has been confirmed by experimentally).

[2] See the "AcousticVNA User's Guide" for more information.

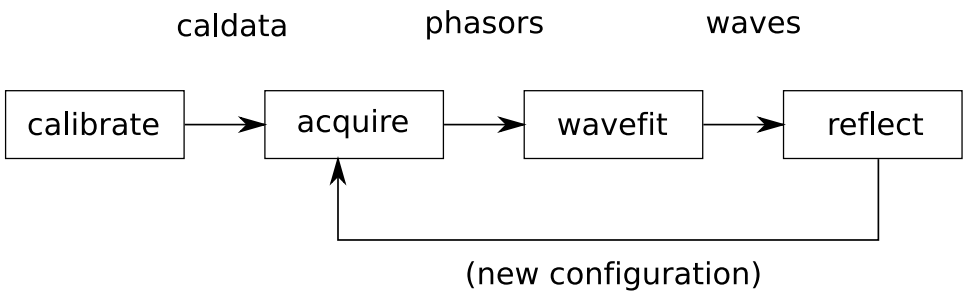

Figure 3.3: Schematic view of the measurement process using the AVNA Lab software (function names are boxed, labels above the arrows indicate data structures passed from one function to the next)

3.2.2 Acquiring data

Following calibration, the microphones are inserted into the microphone section and the test object mounted. A series of sine-wave tones are played through the compression driver at varying frequencies and the microphone signals recorded. The microphone signals are Fourier-transformed to extract the time independent amplitude (or **phasor**) of the driven mode at each microphone. This data is stored as a set of six phasors for each drive frequency. This process is automated by `acquire.m`.

3.2.3 Wave-fitting process

Here we assume that the pressure field in the waveguide may be described by the superposition of left- and right-going plane waves at the drive frequency[3] . Given the complex amplitudes recorded at each microphone, we use a least-squares fitting routine to determine the left- and right-going wave amplitudes, as well as the values of other parameters (including phase velocity and attenuation) that best fit the data. The routine `wavefit.m` carries out the fitting and returns the left- and right-going wave amplitudes at each frequency. This data may be used to calculate useful quantities such as the reflection coefficient at a given reference plane.

[3] Here we must assume that only the (00) mode propagates (see Section 2.2.4). For our waveguide (diameter 2.5 cm) this is always the case below 8 kHz.

Chapter 4

Acoustic Cavities

The study of acoustic resonating cavities is important in a broad range of fields, from musical acoustics to architectural engineering. In many cases, solutions of the Helmholtz equation, using simple sliding boundary conditions, can provide adequate predictions of the properties of a resonating cavity (such as its resonant frequencies). One can obtain accurate numerical solutions of this problem, even for complicated geometries, using a finite-element numerical approach. However, when higher accuracy is needed, or when complications such as fluid viscosity or soft boundaries become important, waveguide measurement techniques may be used to characterize resonances. Because waveguide techniques usually require a modification of the cavity geometry (in order to fit the cavity to a waveguide), they work best when the dimensions of the waveguide are small in comparison to the cavity.

My objective was to use the AcousticVNA apparatus to characterize the resonances of a simple resonating cavity, and then compare the measurements with analytic and numerical calculations. I chose to use a cylindrical cavity because the analysis follows easily from that of the circular waveguide (treated in Section 2.2.4).

Because the cylindrical cavity (and the waveguide to which it is attached) possesses axial symmetry, we expect solutions of the Helmholtz equation to have simple sinusoidal φ dependence:

$$u(\mathbf{r}) = f(r, z) \exp(im\varphi). \tag{4.1}$$

We can thus reduce the problem to a two-dimensional partial differential equation (and tack on φ dependence at the end), making finite-element numerical calculations more feasible.

4.1 What is Resonance?

Roughly speaking, **resonance** occurs when a system is driven at a frequency corresponding to a local maximum in oscillation amplitude. In an acoustic resonating cavity, maximum (acoustic pressure) amplitude is achieved when **standing waves** form inside the cavity, or when the wavelength of the drive signal approaches a dimension of the cavity.

Standing waves have simple sinusoidal time dependence and thus their spatial dependences are solutions of the Helmholtz equation (2.3); we can calculate standing wave patterns in a resonating cavity by solving the Helmholtz equation subject to the appropriate boundary conditions.

4.2 Cylindrical Cavities

4.2.1 Analytic solutions

Consider a cylindrical cavity of radius a and length b. Solving the Helmholtz equation subject to sliding boundary conditions (see Appendix A for a derivation), we arrive at a set of solutions indexed by nonnegative integers n, l and integer m:

$$u_{nml}(r, \varphi, z) = \cos(n\pi z/b) \exp(im\varphi) J_m\left(r\sqrt{k_r^2 - (n\pi/b)^2}\right) \tag{4.2}$$

where

$$k_r^2 = (n\pi/b)^2 + \left(j'_{m,l+1}/a\right)^2. \tag{4.3}$$

(Let $j'_{m\mu}$ be defined as in Section 2.2.2). Given indices n, m, and l, the solution u_{nml} corresponds to a resonance of the cavity, that is, a solution of the wave equation that

satisfies the cavity boundary conditions and has a simple sinusoidal time dependence. From (4.3), we can calculate the frequency corresponding to each resonance (nml) using the relation $f_r = (c/2\pi)\, k_r$.

4.2.2 Experimental characterization

Coupling a cylindrical cavity to the microphone section of the AcousticVNA apparatus allows a measurement of the reflection coefficient at the opening of cavity. The experimental setup is shown in Figure 4.2.

We hypothesize that two phenomena will allow us to use measurements of the reflection coefficient to identify resonances of the cavity:

(1) The magnitude of the reflection coefficient should decrease slightly at a resonance.

(2) The reflection coefficient should undergo a phase shift of 2π (centered at the resonant frequency) near resonance.

In a model that neglects dissipation, the magnitude of the reflection coefficient at a closed, single-port cavity should be identically one. In reality, a fraction of the incident power is transmitted through the cavity walls or converted to heat through friction with surfaces or viscous friction. Such losses increase with the amplitude of pressure oscillation inside the cavity, and thus peak at resonance.

To understand the second effect we must consider the behavior of the pressure field at the cavity opening. Far from resonance, the cavity opening is similar to an open termination—there is a pressure node (minimum) at the opening, requiring that the left- and right-going waves at that point are 180 degrees out of phase. This corresponds to a reflection coefficient of -1. At resonance, however, there is a pressure antinode (maximum) at the cavity opening, corresponding to a reflection coefficient of 1 (because the left- and right-going waves must add in phase). Thus, as we pass by a resonance,

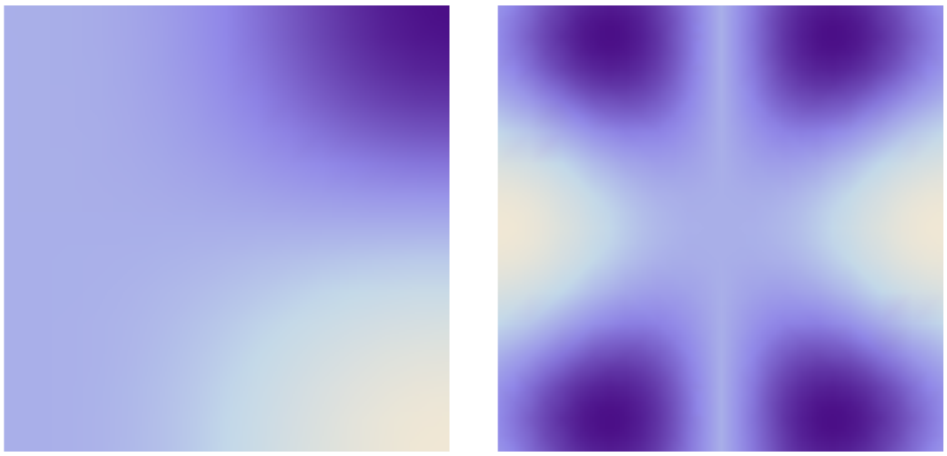

(a) (130) resonance

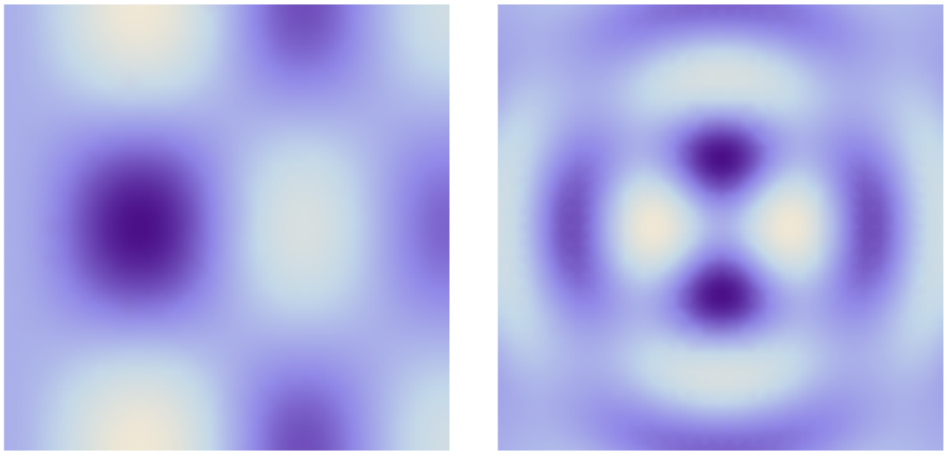

(b) (222) resonance

Figure 4.1: Plots of the pressure field at resonances of a cylindrical cavity (the plots on the left are slices in the xz plane, with the left edge corresponding to $x = 0$ and the right edge $x = a$; the plots on the right are slices in the xy plane at $z = b/2$)

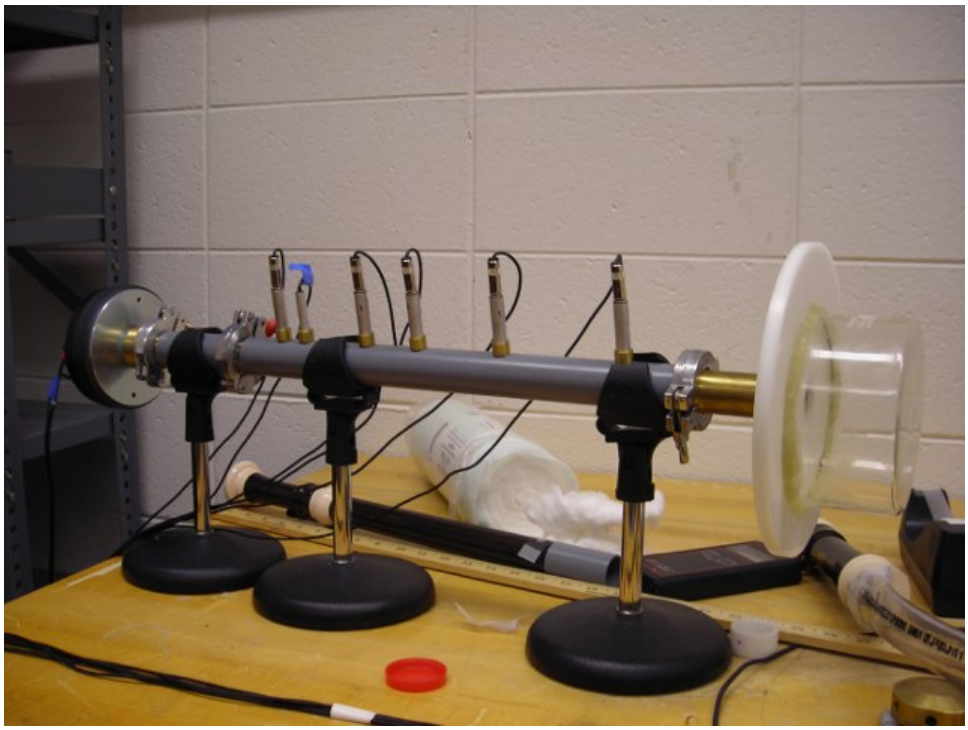

Figure 4.2: AcousticVNA with a cylindrical cavity center-coupled to the microphone section

(nml)	Analytic	Reflectometry ($\pm$50 Hz)
100	2736	2736
110	3208	3198
001	3554	3564
030	3877	3896
101	4436	4478
011	4944	4901
200	5465	5493
210	5626	5627
220	6156	6158

Table 4.1: Comparison of resonant frequencies (in Hz) calculated analytically and estimated by the reflection coefficient (refer to Figure 4.3)

the reflection coefficient goes from 1 to -1 and back to 1, a phase shift of 2π.

The measured reflection coefficient is plotted versus frequency (from 2.5–6.5 kHz) in Figure 4.3. Note that the phase shifts (specifically, points where the phase is changing most quickly) coincide with dropoffs in the magnitude (on the order of 20%) of the reflection coefficient. This seems to suggest that our model is correct, and these points identify resonances of the cavity. Indeed, the frequencies marked by vertical lines in the figure match up fairly closely with those calculated using (4.3) (See Table 4.1 for a comparison of the analytical[1] and experimental results.) Note, however, that there are dropoffs in the reflection coefficient magnitude that do not appear to coincide with phase shifts. Interestingly, these dropoffs coincide with resonances for which $m \neq 0$.

Upon closer examination, we do see a small phase shift near these resonances (see Figure 4.4, for example). Figure 4.4a is particularly useful in understanding why the phase shift is not a full 2π in these cases. The explanation is that the nonzero-m modes are less strongly coupled to the waveguide than are the $m = 0$ modes (intuitively, it is difficult to drive axially-asymmetric modes when the system is axially symmetric). For an example of weak coupling, imagine we were to insert an aperture at the cavity opening. As we make the aperture smaller and smaller, we approach the limit of a

[1] For the calculations I used $c = 343.8$ m/s and the cavity dimensions $a = 5.9$ cm, $b = 6.3$ cm.

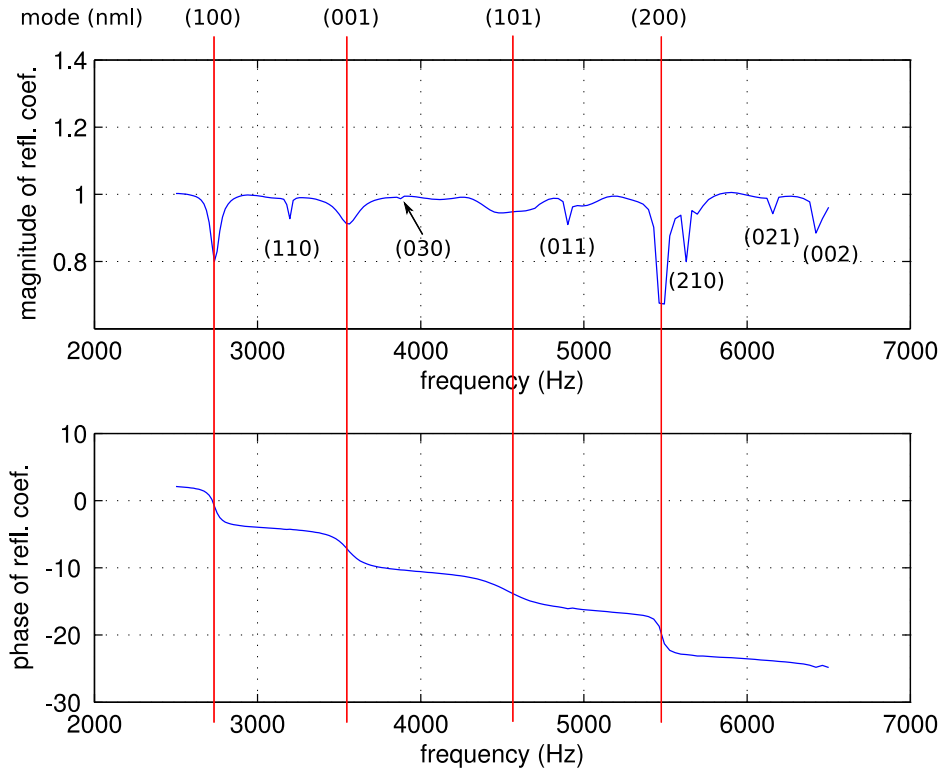

Figure 4.3: Plot of the experimentally-determined reflection coefficient versus drive frequency at the cavity opening (with resonances labeled)

closed end, for which the reflection coefficient is +1. Near a cavity resonance, we would see only a small loop in the overall reflection coefficient (as seen in the figure) because only a small component undergoes the expected 2π phase shift and magnitude dropoff.

We may therefore generalize our second criterion for resonance to read: "There is a loop (i.e. a phase shift of 2π relative to some origin) in the reflection coefficient near resonance."

4.2.3 Numerical modeling

The cavity studied in the experiment is not a perfectly cylindrical, thanks to the opening at which it is connected to the waveguide. In order to carefully analyze the consistency of the waveguide measurements with the predictions of the Helmholtz equation, we need to take into account the slightly more complicated (i.e., including the waveguide as well as the cavity) geometry of the experimental setup. Here an analytic solution is not possible, so we turn to numerical methods.

I utilized MATLAB's numerical PDE toolbox to perform a finite-element solution of the Helmholtz equation, using the geometry shown in Figure 4.5. This geometry represents a slice of the waveguide and attached cylindrical cavity in a plane passing through the axis of symmetry (the solid of rotation obtained by rotating about the horizontal axis in the figure is the true three-dimensional geometry). By fixing m and solving the Helmholtz equation with boundary conditions in this simplified geometry, we may determine the r and z dependence in (4.1).

We used sliding boundary conditions at the surfaces of the waveguide and cavity, and the **matched driver** boundary condition at the driver end of the waveguide. The matched driver condition requires that

$$\hat{\mathbf{z}} \cdot \nabla u = ik\,(2 - u) \text{ at } z = 0. \tag{4.4}$$

This is the sliding condition with a forcing term, which represents the driver. The

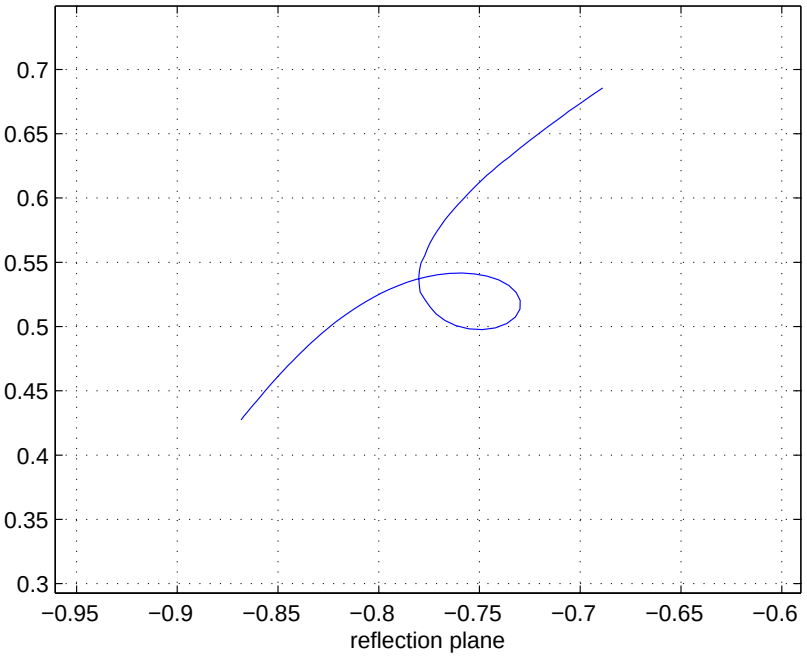

(a) Reflection coefficient plotted on the complex plane

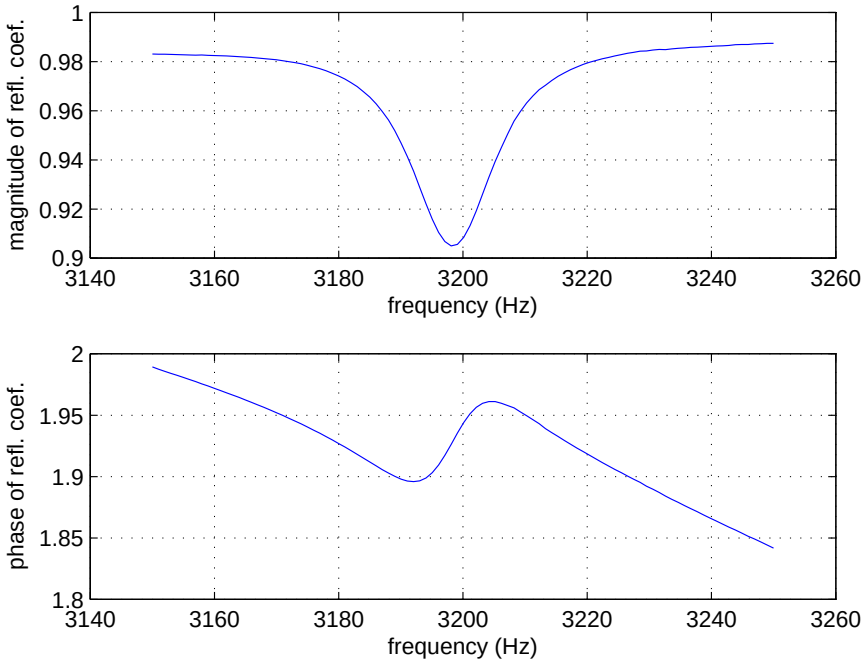

(b) Magnitude and phase of the reflection coefficient

Figure 4.4: Plots of the reflection coefficient near the second $m = 1$ resonance (110)

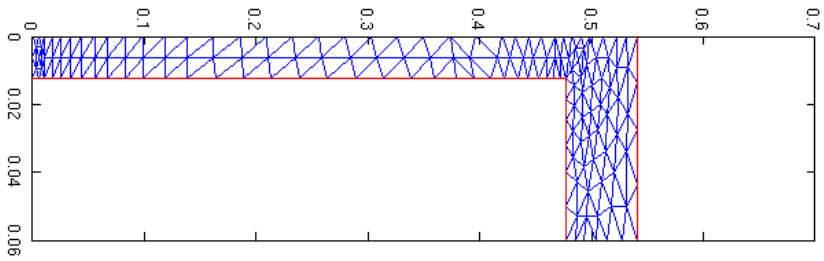

Figure 4.5: Two-dimensional geometry and mesh used in the finite-element numerical calculations (scale is meters)

form of the forcing term ensures that the magnitude of the wave propagating in the $+z$ direction (away from the driver) is always 1, which allows us to focus on resonances of the cavity rather than those of the cavity-waveguide system.

By varying k in (4.4), I produced a series of finite-element calculations of the pressure field in the waveguide at various drive frequencies. From this data I extracted complex amplitudes of the pressure field at the microphone locations, and used `wavefit.m` to fit right- and left-going waves. These data allowed me to plot the reflection coefficient versus frequency, shown in Figure 4.7.

The experimental and numerical phases match almost perfectly. The only noticeable inconsistency, a horizontal stretching of the experimental curve when compared with the numerical one, can be explained by the fact that the phase velocity of sound within the waveguide varies with frequency (from about 343.6–344 m/s in this range), while we use a fixed phase velocity in the numerical calculation. The magnitudes we do not expect to agree, as the numerical calculation does not account for losses.

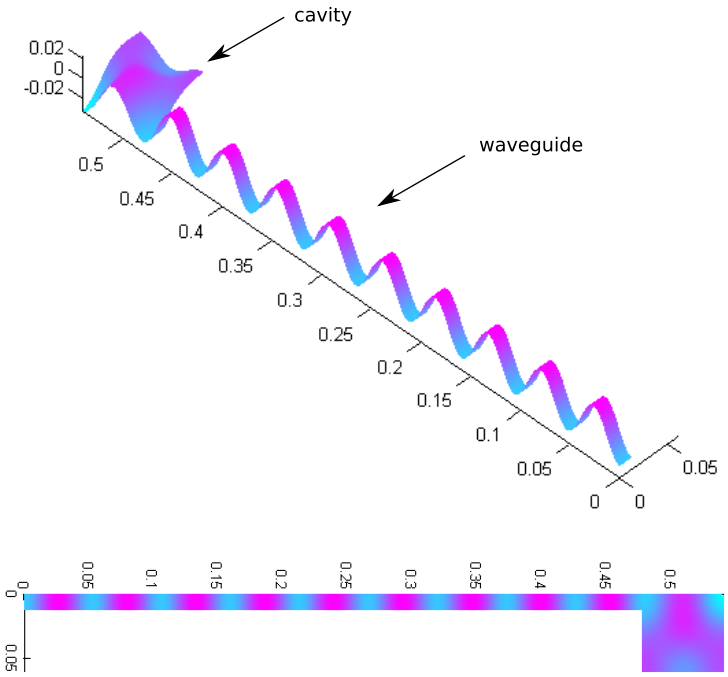

Figure 4.6: Finite-element numerical solution of the pressure field inside the waveguide and cavity for a drive frequency of 6080 Hz, near the resonant frequency of the (201) mode (units of pressure are arbitrary)

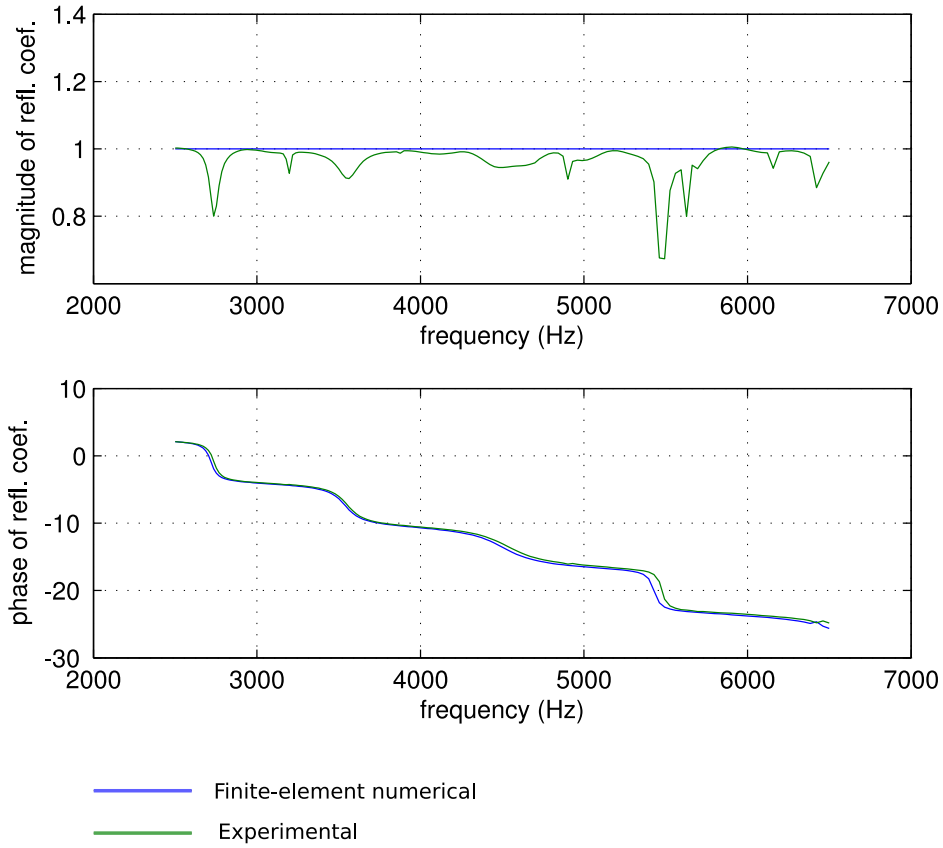

Figure 4.7: The plot of reflection coefficient versus frequency obtained through numerical solution of the Helmholtz equation is in excellent agreement with the measurements.

Chapter 5

Multi-Port Measurements and Future Directions

With the addition of a second microphone section, the existing AcousticVNA hardware can (in theory) be used as a two-port vector network analyzer (see Figure 5.1). Most of my recent work has been in extending the AVNA Lab software to support an arbitrary number of ports and microphone channels. I have been partially successful: I have designed and implemented a scheme for relatively calibrating an arbitrary number of microphones, extended the wave-fitting procedure to simultaneously determine modal amplitudes in an arbitrary number of ports, and written a program for the calculation and visualization of s-matrix elements.

5.1 Calibration and Wave-Fitting for n Ports

Two-port measurements using AcousticVNA require the relative calibration of twelve microphones (six per microphone section), which is slightly tricky business because the standard calibration cell (Figure 3.2) only accommodates six microphones. To circumvent this issue we run the calibration routine multiple times, each time swapping out all but one microphone (the reference mic) until all have had their turn in the cell. The relative amplitudes obtained at each stage are multiplied by the factor that makes the amplitude of the reference microphone equal to one. This process is automated by the new routine `supercal.m`.

Multi-port analysis requires a modification of the wave-fitting procedure. Initially

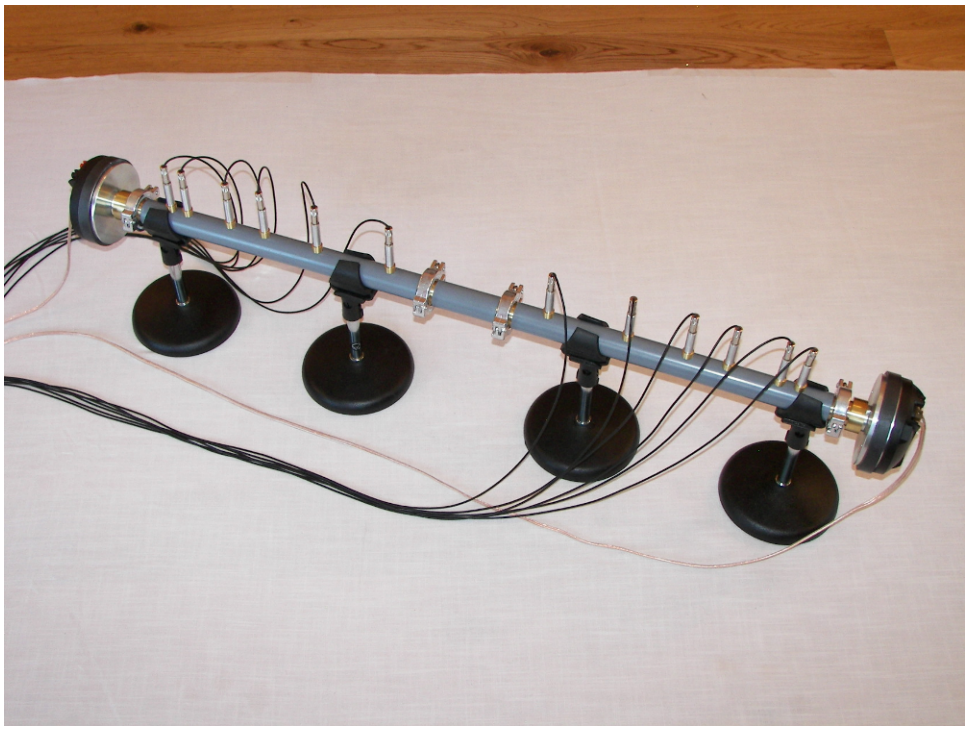

Figure 5.1: The AcousticVNA system configured as a two-port vector network analyzer

we decided that the best option would be to modify the existing code to fit right- and left-going amplitudes in all ports simultaneously, treating the phase velocity of sound and the attenuation constant as global parameters. This method turned out to be more difficult to implement than I had expected, and has not yet produced accurate results (almost certainly due to bugs in the code). In retrospect, it would have been easier to perform a separate fit in each port; although fitting to global parameters might have produced more accurate results (because the microphone sections are essentially identical), a separate fit would be easier to implement and would allow for small differences between microphone sections.

5.2 Scattering Matrix Calculation

In a two-port system, the scattering matrix has four elements—to determine these elements we will need four linear equations. Our algorithm is as follows:

(1) Drive (play a tone through the driver) the first port. Record the right- and left-going amplitudes in each port. Using these amplitudes we can write two linear equations:

$$\begin{pmatrix} b_1 \\ b_2 \end{pmatrix} = S \begin{pmatrix} a_1 \\ a_2 \end{pmatrix}.$$

(2) Drive the second port. Record amplitudes a_i' and b_i'. Now,

$$\begin{pmatrix} b_1' \\ b_2' \end{pmatrix} = S \begin{pmatrix} a_1' \\ a_2' \end{pmatrix}.$$

(3) Determining the s-matrix now amounts to solving a pair of two-dimensional linear systems:

$$\begin{pmatrix} a_1 & a_2 \\ a_1' & a_2' \end{pmatrix} \begin{pmatrix} s_{11} \\ s_{12} \end{pmatrix} = \begin{pmatrix} b_1 \\ b_1' \end{pmatrix}$$

and

$$\begin{pmatrix} a_1 & a_2 \\ a_1' & a_2' \end{pmatrix} \begin{pmatrix} s_{21} \\ s_{22} \end{pmatrix} = \begin{pmatrix} b_2 \\ b_2' \end{pmatrix}.$$

This algorithm can be easily implemented in MATLAB by making use of built-in linear algebra capabilities (see `smatrix.m`).

5.3 Future Directions

My most immediate goal is to re-implement the multi-port wave-fitting routine to perform a separate fit at each port. When this is complete, I would like to fix the problems with the current global fitting method and compare results obtained using the two methods.

Once we have a reliable method of determining the scattering matrix, I would like to perform several preliminary experiments for which the theory is well-understood—this will allow us to test the accuracy of our scattering matrix measurements. One such experiment would be to measure the scattering matrices of waveguide apertures of different sizes—such a configuration is easily modeled using numerical PDE software.

Bibliography

[1] M. Abromowitz and I.E. Stegun. Handbook of Mathematical Functions. National Bureau of Standards, 1972.

[2] Arthur H. Benade. Fundamentals of Musical Acoustics. Oxford University Press, London, 1976.

[3] Neville H. Fletcher and Thomas D. Rossing. The Physics of Musical Instruments. Springer-Verlag, New York, 1991.

[4] D.M. Kerns and R.W. Beatty. Basic Theory of Waveguide Junctions and Introductory Microwave Network Analysis. Pergamon Press, London, 1967.

[5] C.A. Lee and G.C. Dalman. Microwave Devices, Circuits, and Their Interaction. John Wiley and Sons, New York, 1994.

[6] Daniel McKinnon. Acoustics of the Tenor Recorder. PhD thesis, University of Colorado at Boulder, 2009.

[7] Allan D. Pierce. Acoustics: An Introduction to Its Physical Principles and Applications. McGraw-Hill, New York, 1981.

[8] John Price. Acoustic Waveguides. University of Colorado, Boulder, 2008.

[9] John Price. AcousticVNA User's Guide. University of Colorado, Boulder, 2008.

[10] Minhong Rim and Yang-Hann Kim. Narrowband noise attenuation characteristics of in-duct acoustic screens. Journal of Sound and Vibration, 234:737–759, 2000.

[11] S. Thwaites and N.H. Fletcher. Acoustic and aerodynamic determinants of the sound quality of flutes. Acoustical Society of America, 74:400–408, 1983.

[12] J.P.M. Trusler. Physical Acoustics and Metrology of Fluids. Taylor and Francis, New York, 1991.

Appendix A

Modes of a Cylindrical Cavity

The analysis of circular waveguides in Section 2.2.4 can be extended to a simple cylindrical cavity by imposing the additional boundary condition:

$$\hat{\mathbf{z}} \cdot \nabla p = 0 \text{ at } z = 0,\, b. \tag{A.1}$$

Taken together, boundary conditions (2.16) and (A.1) describe a closed cylinder of length b oriented along the z axis. Looking back to (2.4), the boundary condition (A.1) is equivalent to

$$g'(0) = g'(b) = 0.$$

The first condition enforces that $a = b$ in (2.8), that is, the amplitude of the wave propagating in the $+z$ direction is equal to the amplitude of the wave propagating in the $-z$ direction.

The second condition leads to quantization of the propagation constant, γ. Note that in order to satisfy $g'(b) = 0$, γ must be an integral multiple of π/b.

We can now write the modal z dependence

$$g_n(z) = \cos(n\pi z/b),\ n \in \mathbb{Z}. \tag{A.2}$$

Combining (A.2) with (2.17) and (2.18), we can write the complete modal solution, labeled by nonnegative integers n and l and integer m:

$$u_{nml}(r, \varphi, z) = \cos(n\pi z/b) \exp(im\varphi) J_m\left(r\sqrt{k_r^2 - (n\pi/b)^2}\right).$$

where (using the definition of $j'_{m\mu}$ introduced in Section 2.2.4)

$$k_r^2 = (n\pi/b)^2 + \left(j'_{m,l+1}/a\right)^2 .$$